HHS Public Access

Author manuscript

Bioconjug Chem. Author manuscript; available in PMC 2021 July 15.

Published in final edited form as:

Bioconjug Chem. 2020 July 15; 31(7): 1844–1856. doi:10.1021/acs.bioconjchem.0c00342.

Complement Inhibitors Block Complement C3 Opsonization and Improve Targeting Selectivity of Nanoparticles in Blood

Hanmant Gaikwad,
Translational Bio-Nanosciences Laboratory, Department of Pharmaceutical Sciences, The Skaggs School of Pharmacy and Pharmaceutical Sciences, and Colorado Center for Nanomedicine and Nanosafety, University of Colorado Anschutz Medical Campus, Aurora, Colorado 80045, United States

Yue Li,
Translational Bio-Nanosciences Laboratory and Department of Pharmaceutical Sciences, The Skaggs School of Pharmacy and Pharmaceutical Sciences, University of Colorado Anschutz Medical Campus, Aurora, Colorado 80045, United States

Geoffrey Gifford,
Translational Bio-Nanosciences Laboratory and Department of Pharmaceutical Sciences, The Skaggs School of Pharmacy and Pharmaceutical Sciences, University of Colorado Anschutz Medical Campus, Aurora, Colorado 80045, United States

Ernest Groman,
Translational Bio-Nanosciences Laboratory, Department of Pharmaceutical Sciences, The Skaggs School of Pharmacy and Pharmaceutical Sciences, and Colorado Center for Nanomedicine and Nanosafety, University of Colorado Anschutz Medical Campus, Aurora, Colorado 80045, United States

Nirmal K. Banda,
Division of Rheumatology, School of Medicine, University of Colorado Anschutz Medical Campus, Aurora, Colorado 80045, United States

Laura Saba,

Corresponding Authors: Guankui Wang – Translational Bio-Nanosciences Laboratory, Department of Pharmaceutical Sciences, The Skaggs School of Pharmacy and Pharmaceutical Sciences, and Colorado Center for Nanomedicine and Nanosafety, University of Colorado Anschutz Medical Campus, Aurora, Colorado 80045, United States; guankui.wang@cuanschutz.edu; Dmitri Simberg – Translational Bio-Nanosciences Laboratory, Department of Pharmaceutical Sciences, The Skaggs School of Pharmacy and Pharmaceutical Sciences, and Colorado Center for Nanomedicine and Nanosafety, University of Colorado Anschutz Medical Campus, Aurora, Colorado 80045, United States; dmitri.simberg@ucdenver.edu.

Complete contact information is available at: https://pubs.acs.org/10.1021/acs.bioconjchem.0c00342

Supporting Information

The Supporting Information is available free of charge at https://pubs.acs.org/doi/10.1021/acs.bioconjchem.0c00342.

Table S1, Characterization of double labeled particles used in Figure 2; Table S2, statistical analysis for Figure 4; Table S3, statistical analysis for Figure 6; Figure S1, uptake by control cells that do not express EpCAM and Her2/neu; Figure S2, effect of antibody/NP number on targeting efficiency; Figure S3, accumulation of targeted CLIO NWs in SKBR3 cells after incubation at different concentrations in whole blood; Figure S4, identification of DiR labeled SKBR3 cells and leukocytes in lysed blood; and Figure S5, inhibition of leukocyte uptake and no effect on SKBR3 uptake of CLIO NWs (10 μg/mL) by complement inhibitors (PDF) Standard curve data (XLS)

The authors declare no competing financial interest.

Systems Genetics and Bioinformatics Laboratory and Center for Translational Pharmacokinetics and Pharmacogenomics, University of Colorado Anschutz Medical Campus, Aurora, Colorado 80045, United States

Robert Scheinman,
Department of Pharmaceutical Sciences, The Skaggs School of Pharmacy and Pharmaceutical Sciences and Colorado Center for Nanomedicine and Nanosafety, University of Colorado Anschutz Medical Campus, Aurora, Colorado 80045, United States

Guankui Wang,
Translational Bio-Nanosciences Laboratory, Department of Pharmaceutical Sciences, The Skaggs School of Pharmacy and Pharmaceutical Sciences, and Colorado Center for Nanomedicine and Nanosafety, University of Colorado Anschutz Medical Campus, Aurora, Colorado 80045, United States;

Dmitri Simberg
Translational Bio-Nanosciences Laboratory, Department of Pharmaceutical Sciences, The Skaggs School of Pharmacy and Pharmaceutical Sciences, and Colorado Center for Nanomedicine and Nanosafety, University of Colorado Anschutz Medical Campus, Aurora, Colorado 80045, United States;

Abstract

Complement is one of the critical branches of innate immunity that determines the recognition of engineered nanoparticles by immune cells. Antibody-targeted iron oxide nanoparticles are a popular platform for magnetic separations, in vitro diagnostics, and molecular imaging. We used 60 nm cross-linked iron oxide nanoworms (CLIO NWs) modified with antibodies against Her2/neu and EpCAM, which are common markers of blood-borne cancer cells, to understand the role of complement in the selectivity of targeting of tumor cells in whole blood. CLIO NWs showed highly efficient targeting and magnetic isolation of tumor cells spiked in lepirudin-anticoagulated blood, but specificity was low due to high uptake by neutrophils, monocytes, and lymphocytes. Complement C3 opsonization in plasma was predominantly via the alternative pathway regardless of the presence of antibody, PEG, or fluorescent tag, but was higher for antibody-conjugated CLIO NWs. Addition of various soluble inhibitors of complement convertase (compstatin, soluble CD35, and soluble CD55) to whole human blood blocked up to 99% of the uptake of targeted CLIO NWs by leukocytes, which resulted in a more selective magnetic isolation of tumor cells. Using well-characterized nanomaterials, we demonstrate here that complement therapeutics can be used to improve targeting selectivity.

INTRODUCTION

Antibody-decorated superparamagnetic iron oxide (SPIO) nanoparticles hold an important niche in biomedical research and nanomedicine. On the one hand, they have been successfully utilized for magnetic isolation of a variety of targets, including immune cells and circulating tumor cells from blood and cell suspensions, as well as molecular targets in pulldown assays.[1,2] Immunomagnetic isolation is frequently used in clinical procedures and assays, for example, in the production of Chimeric Antigen Receptor (CAR)-T cells[3] and for

analysis of circulating tumor cells (CTCs).[4] On the other hand, due to high magnetic resonance imaging contrast properties,[2,5] there is a considerable interest in using iron oxide particles targeted to disease markers for molecular imaging.[6]

Dextran-coated SPIO has been used clinically in patients as an MRI contrast agent and iron supplement, in part due to the scalability and low cost of synthesis.[2] Cross-linking the dextran coat with epichlorohydrin leads to the formation of three-dimensional hydrogel coated iron oxide (termed CLIO) with important chemical and biochemical properties: (a) cross-linked hydrogel improves NP stability in plasma and prolongs circulation time in mice;[7,8] and (b) residual epoxy groups can be used for further functionalization of CLIO with amines, fluorophores, peptides, and antibodies. CLIO has been functionalized with radioisotopes, fluorophores, and sensor modules, which targeted antibodies for diagnostic and theranostic applications in cancer, inflammation, diabetes, and atherosclerosis.[6,9–11] While CLIO represents an impressive and highly versatile platform for in vivo imaging, and notwithstanding the success in preclinical mouse studies, there is a gap in the fundamental understanding of how surface functionalization of CLIO with antibodies and imaging molecules affects immune recognition in humans. Targeting specificity of NPs is usually validated by comparing antibody conjugated and control formulations, and using the cells with and without the targeting marker.[12–14] However, another level of specificity, which is often overlooked for targeted nanoparticles, is the level of uptake by immune cells.[15,16] It is highly important to reduce nonspecific recognition of targeted nanoparticles by immune cells to improve target/background ratio and specificity,[15,17] but the strategies to avoid immune uptake are mostly limited to modifications of surface chemistry.

Complement is the critical arm of serum innate immunity responsible for neutralization of foreign pathogens. The exposure of foreign surfaces to serum results in a rapid generation of C3 and C5 convertases that promote opsonization through covalent attachment of C3b and the formation of anaphylatoxins (e.g., C3a and C5a).[18] C3b and its cleavage products iC3b, C3dg, and C 3d promote recognition by complement receptors on neutrophils, monocytes, eosinophils, lymphocytes, erythrocytes, and resident tissue macrophages.[19–21] Complement is one of the factors negatively affecting the hemocompatibility of nano- and biomaterials. Many reports have shown complement activation by nanoassemblies including carbon nanotubes,[22,23] micelles,[24] liposomes,[25] polymeric nanospheres,[26,27] gold NPs,[28] and SPIO.[29] Here, we used previously described elongated CLIO nanoworms (CLIO NWs)[7] to understand the involvement of complement in immune recognition of targeted iron oxides in humans. The easiest way to test hemocompatibility in different human subjects is to use donated anticoagulated blood. Lepirudin (recombinant hirudin) is the selective inhibitor of thrombin and to our knowledge is one of the few anticoagulants that does not interfere with complement activation, as compared to EDTA or citrate.[30] CLIO NWs were modified with antibodies against tumor cell marker Her2/neu (over 20% of breast cancers[31]) and EpCAM (epithelial marker on circulating tumor cells[32]) and were rigorously characterized to correlate the composition to the biological outcome. Our results suggest that the alternative pathway plays the predominant role in the complement C3 opsonization regardless of surface functionalization and that addition of specific complement inhibitors can dramatically improve targeting selectivity in human blood. This study introduces a novel

notion of using complement inhibitors for improving stealth properties and the selectivity of targeted nanomaterials.

RESULTS

CLIO NWs Show High Targeting Efficiency in BSA and Plasma.

We used dextran SPIO NWs (62 nm, ζ −5 mV, Table 1)[33,34] to synthesize cross-linked CLIO NWs (51 nm, ζ −5 mV, Table 1) by a modified "harsh" cross-linking method[7,8] (see Methods). The cross-linked CLIO NWs were aminated by reacting the residual epoxy groups of epichlorohydrin with ammonia (56 nm, ζ +15 mV, Table 1).

To conjugate antibodies, we employed copper-free Diels–Alder click addition of strained *trans*-cyclooctene (TCO) and methyltetrazine (MTZ). This reaction is highly versatile due to very fast second-order kinetics and high stability of the resulting bond.[35] In the first step (Figure 1, step 1), CLIO NWs-NH_2 were reacted first with a 100-fold molar excess of fluorescent dye (Cy5-NHS or Cy3-NHS), followed by carbodiimide conjugation of MTz-PEG3400-COOH (2000-fold molar excess). Acetyl groups were used to block the residual amines, which resulted in particles with slightly negative zeta-potential (Table 1). The particles were further conjugated with TCO-modified anti-Her2/neu or anti-EpCAM antibodies (Figure 1, steps 2–3). The addition of a 100-fold molar excess of the antibody resulted in 75 Her2/neu Abs and 60 EpCAM Abs per Cy5-labeled NP (see Table 1 and supplemental data for Ab/NP quantification).

In addition, we prepared nonlabeled CLIO NWs with 72 anti-Her2/neu Ab/NP and 57 anti-EpCAM Ab/NP (Table 1), and Cy3-labeled CLIO NWs with 75 anti-Her2/neu-Cy5 Ab/NP and 54 anti-EpCAM-Cy5 Ab/NP (Table S1). The size and zeta potential were not changed by the dye conjugation, but the size was increased by ~4 nm after Ab conjugation (Table 1). According to flow cytometry analysis (Figure 2A), both Cy5-CLIO NWs-PEG-Her and Cy5-CLIO NWs-PEG-EpCAM (0.1 μg Fe/mL to 100 μg/mL) showed efficient binding to SKBR3 tumor cells in the presence of 10 mg/mL BSA (Figure 2B). Nontargeted Cy5-CLIO NWs-PEG-MTz showed some binding at 100 μg Fe/mL, but it was 30–60 times lower than the targeted NPs (Figure 2A,B). Both types of targeted NPs showed no uptake by MDA MB-231 cells, which do not express EpCAM and Her2/neu[36] (Figure S1). The preparations with lower Ab/NP ratios (25 and 32) showed less efficient uptake by SKBR3 cells (Figure S2); therefore, we used targeted NWs with higher ratios for all subsequent binding studies. Both types of targeted particles showed an increase in binding from 0.2 to 20 μg Fe/mL (Figure 2C,D) in 10 mg/mL BSA and in lepirudin-anticoagulated human plasma, and the targeting efficiency in BSA and plasma was similar (Figure 2E), which suggests that the plasma protein "corona" does not interfere with the targeting.

To track intracellular accumulation of NPs and tethered Abs, we used CLIO NWs labeled with Cy3 and conjugated with Cy5-labeled anti-Her2/neu or anti-EpCAM Ab. Confocal microscopy showed that SKBR3 cells internalized both Cy3-CLIO NWs-PEG-Her-Cy5 and Cy3-CLIO NWs-PEG-EpCAM-Cy5 and there was a colocalization of NPs and Abs (Figure 2F).

CLIO NWs Show High Leukocyte Uptake in Whole Blood, Which Decreases Targeting Selectivity.

Targeting with CLIO NWs in BSA and plasma was highly selective; i.e., the uptake was antibody dependent, and there was no uptake by receptor-negative cells. Nonspecific uptake of iron oxide nanoparticles is one of the most serious drawbacks of immunomagnetic capture, especially for analysis of circulating tumor cells (CTCs).[37–40] To test the targeting and uptake in whole blood, SKBR-3 cells were prelabeled with a lipophilic membrane dye DiR and spiked at 100 000 cells/mL blood, followed by Cy3-CLIO NWs-PEG-Her-Cy5 or Cy3-CLIO NWs-PEG-EpCAM-Cy5 at 0.1, 1, and 10 μg Fe/mL. Following incubation for 15′, the intracellular particles were readily detectable inside blood-borne tumor cells (Figure 3A for 1 μg/mL and Figure S3), which suggests fast and sensitive targeting in blood. We spiked lepirudin-anticoagulated blood from healthy donors with ~18 DiR-labeled SKBR cells per 5 mL, followed by CLIO NWs-PEG-Her. After the blood was passed through a MACS column, magnetic cells were eluted and captured on a nitrocellulose membrane (Figure 3B). High-resolution near-infrared scanning showed approximately 60% efficiency of recovery of DiR-labeled spiked cells (Figure 3C). At the same time, immunostaining of CLIO NWs-PEG-Her-isolated cells with CD45 showed a large number of contaminating leukocytes eluted from the MACS column (Figure 3D).

Flow cytometry analysis of magnetically labeled cells demonstrated large numbers of neutrophils, monocytes, lymphocytes, and erythrocytes (Figure 3E), similar to our previous observations using larger 110 nm SPIO NWs and nontargeted CLIO NWs.[20,41] For those larger particles, we previously found the leukocyte uptake to be almost entirely complement-dependent.[20,41] EDTA is the universal inhibitor of all complement activation pathways. We performed the same experiment in matched EDTA anticoagulated blood and found a dramatic decrease in the number of magnetic leukocytes (Figure 3E).

Specific Inhibition of Complement Improves Selectivity.

To investigate the involvement of the complement system in the uptake of CLIO NWs and to determine the activation pathway as a function of surface chemistry, we measured the level of C3 deposition for all nanoparticles listed in Table 1 in lepirudin plasma from three different donors (one female and two males). We used 10 mM EGTA/Mg^{2+} to inhibit calcium-sensitive classical and lectin pathways (CP and LP, respectively), 10 mM EDTA to inhibit all pathways, and 125 μg/mL of C1INH to inhibit the classical pathway (Figure 4A).

According to Figure 4B, all antibody-conjugated CLIO NWs showed significantly higher C3 deposition as compared to control CLIO NWs-PEG-MTz (p-value < 0.0001 for all targeted particles vs control, with or without Cy5, Table S2). Labeling with Cy5 did not cause a significant change in C3 deposition on the particles (p-value > 0.1 for all particles). C1INH did not cause a significant decrease in C3 deposition on the particles (Figure 4B, p-value > 0.1 for all particles), whereas EGTA/Mg caused a significant decrease only for CLIO NWs-PEG-Her (Figure 4B, p-value = 0.0001). These data suggest that all particles activate complement predominantly via the AP, but exclude the role of the CP. These data also corroborate our previous findings that modifications of the nanoworms' surface do not decrease complement activation.[34] The reason for this is not necessarily the chemistries, but

the protein corona that always absorbs to the surface and provides binding sites for C3.[42] Interestingly, even in the presence of 10 mM EDTA, there was ~30% of C3 left on antibody-conjugated CLIO NWs. The reason for the incomplete inhibition was not investigated but could be due to the binding of nascent C3b or hydrolyzed C3(H_2O) to antibody-modified NWs in a convertase-independent manner. Indeed, the ability of IgG to bind C3b and to seed complement activation has been demonstrated previously.[43–45]

Complement control proteins (CCPs) are well-characterized natural complement regulators[46] that consist of multiple domains called short consensus repeats (SCRs) or "sushi" domains of about 60–70 amino acids each. CD55 (decay-accelerating factor) is a glycosylphosphatidylinositol-anchored protein,[46] and CD35 (complement receptor 1, CR1) is a transmembrane protein,[47] while factor H is a serum protein (Figure 5A).

These proteins bind to C3b and lead to a disassembly (decay) of the AP convertase (Figure 5B, left). Another complement inhibitor Cp40 (compstatin) is a small cyclic peptide (Figure 5A) that binds noncleaved C3 and blocks its cleavage by convertases (Figure 5B, right).[50] We previously found that compstatin and the first three N-terminal SCR domains of CD55 (soluble CD55, Figure 5A) potently inhibit complement C3 opsonization of different nanoparticles with high nanomolar to low micromolar IC_{50} values.[41] We used a soluble CR1 construct that contains the first 10 N-terminal SCRs of CR1 (sCR1, Figure 5A[51]) to measure the IC_{50} of C3 deposition on nontargeted and targeted CLIO NWs. According to Figure 5C, sCR1 showed low- to mid-nanomolar IC_{50} values in two plasma donors (one male and one female). Notably, while the opsonization of CLIO NWs-PEG-MTZ with C3 was completely inhibited, between 17% and 38% of C3 still remained bound to antibody-conjugated CLIO NWs even at micromolar concentrations, which again confirms that some of the C3 binds to the antibody-coated nanoparticles in convertase-independent fashion.

Next, we studied the ability of sCD55, sCR1, and Cp40 to block the leukocyte uptake of anti-Cy5-CLIO-NWs-PEG-MTz, Cy5-CLIO-NWs-PEG-EpCAM, and Cy5-CLIO-NWs-PEG-Her (2 μg/mL blood). Because the levels of leukocyte uptake in a general population are variable,[41] we used the blood of four healthy donors, two males and two females. According to flow cytometry analysis of blood after RBC lysis (Figure 6A,B), sCD55, Cp40, and sCR1 significantly affected the leukocyte uptake of all nanoparticles (ANOVA main effect of inhibitors p-value = 2.8×10^{-15}, Table S3).

Using post hoc testing, all three inhibitors significantly decreased leukocyte uptake as compared to control in all three CLIO NW types. The only exception was the comparison between sCD55 and control for Cy5-CLIO-PEG-MTz where there was a decrease in leukocyte uptake, but it did not reach statistical significance (p-value = 0.24). In some subjects, Cp40 and/or sCR1 blocked the uptake by up to 99% (Figure 6B). A separate aliquot of lepirudin blood was spiked with DiR-labeled SKBR3 cells (100 000/mL), followed by the particles (2 μg/mL). The inhibitors did not affect the uptake of CLIO NWs by SKBR3 (ANOVA main effect of inhibitors p-value = 0.23; ANOVA interaction effect p-value > 0.99), although there was a significant difference in uptake between particles (ANOVA main effect of particle type p-value = 4.1×10^{-10}; Figure 7A,B, Figure S4 for gating of tumor cells). In this comparison, expectably, Cy5-CLIO-PEG-EpCAM and Cy5-

CLIO-PEG-Her had a significantly higher uptake than did Cy5-CLIO-PEG-MTz (p-value < 0.001 for all comparisons). The same results were observed for 10 μg/mL of CLIO NWs with the inhibitors (Figure S5).

Last, we tested the purity of MACS-isolated SKBRs using Cp40. We added 10 μg/mL of Cy5-CLIO NWs-PEG-Her and 30 μg/mL of Cp40 to lepirudin blood spiked with ~30 SKBR3 cells/mL, isolated cells with MACS as described in Figure 3, and analyzed the magnetically isolated cells after immunostaining for cytokeratin and CD45. Addition of Cp40 reduced the number of magnetic CD45+/DAPI+ leukocytes, which resulted in relatively pure isolated tumor cells (Figure 7C). We used flow cytometry to measure the number and mean fluorescence of magnetically labeled leukocytes after elution of the cells from MACS column with or without the inhibitor. The number of eluted leukocytes (per 30 μL of eluate) and Cy5 fluorescence of magnetically labeled leukocytes was decreased by 80–90% in Cp40 and 10 mM EDTA blood for nontargeted and targeted CLIO NWs (Figure 7D).

CONCLUSIONS

We prepared and characterized 60 nm CLIO NWs with controlled modifications on the surface: cross-linking, amination, PEGylation, fluorescent labeling, and two different humanized monoclonal antibodies. CLIO NWs showed efficient and sensitive targeting of tumor cells in BSA, plasma, and blood. Despite that, specificity was compromised due to complement-dependent immune uptake by blood leukocytes. We further measured complement C3 opsonization and found that, regardless of the surface chemistry, all formulations were opsonized with C3 via the AP. Antibody conjugation generally enhanced complement activation, but there was no involvement of the CP in C3 opsonization of these particles. Complement played a predominant role in the uptake by blood leukocytes. To our knowledge, this is the first report in that synthetic complement inhibitors significantly improved the targeting selectivity in human blood. C3b can covalently bind to immunoglobulins on the NP surface,[45] and C3 opsonization could theoretically inhibit the antibody function. However, we did not observe differences in targeting in BSA versus plasma, which suggested that C3 binding to particles does not affect the targeting efficiency.

Biocompatibility and selectivity are the critical issues of nanomedicines.[52,53] Complement therapeutics is a highly active field in pharmaceutical development, due to the ubiquitous role in many diseases and abundance of druggable proteolytic targets.[54,55] Our research demonstrates a novel approach that can be applied to improve hemocompatibility and selectivity of nanomaterials. Further experiments will be needed to elucidate the feasibility and safety of this approach in vivo.

MATERIALS

Chemicals used for CLIO NW synthesis, including iron salts, epichlorohydrin 10 kDa bifunctional hydroxy PEG, and 12–25 kDa dextran, were purchased from Sigma-Aldrich (St. Louis, MO). NH_2-PEG3400-VA was from Laysan Bio (Arab, AL). TCO-PEG_4-NHS, MTz-Cy3, and MTz-NHS were obtained from Click Chemistry Tools (Scottsdale, AZ). EDC (1-

ethyl-3-(3-(dimethylamino)propyl) carbodiimide hydrochloride) was from Chem-Impex Int'l, Inc., and sulfosuccinimidyl acetate was from Thermo Fischer. The nanoparticle size distribution and zeta potential were measured using a Malvern Zeta Sizer Nano ZS (Malvern Instruments, U.S.). Cy5 and Cy3 NHS esters were from Lumoprobe. DiR (1,1′-dioctadecyl-3,3,3′,3′-tetramethylindotricarbocyanine iodide) was from Biotium (Hayward, CA) and was stored as 2 mM stock in ethanol. Zeba Spin Desalting Columns were purchased from Thermo Fisher Scientific. Bovine serum album was from Sigma-Aldrich. Anti-human EpCAM (epithelial cell adhesion molecule) antibody ING-1[56] was provided by XOMA Corp. (Emeryville, CA). HERCEPTIN (trastuzumab, hereafter), the anti-human Her2/neu antibody (hereafter Her), was obtained from the pharmacy of the University of Colorado Hospital. Alexa Fluor 488 mouse anti-pan Cytokeratin antibody (clone AE1/AE3) was purchased from eBioscience (San Diego, CA). Alexa Fluor 594 mouse anti-CD45 was purchased from BioLegend (San Diego, CA). BD Cytofix/Cytoperm kit was purchased from BD Biosciences (San Diego, CA). DAPI/antifade mounting media were from Vector Laboratories. Nitrocellulose membrane (0.45 μm pore) was from Bio-Rad. MACS Midi column was Miltenyi Biotech. Human leupuridin and K2 EDTA whole blood were obtained from consented healthy donors at the University of Colorado Blood Donor Center under the Center's Institutional Review Board protocol for anonymous collection as described previously;[42] only age and gender were made available to the investigators. Mouse anti-human C3 was from Quidel Corp. (San Diego, CA). Secondary goat anti-mouse IgG labeled with IRDye 800CW was from Li-COR Biosciences (Lincoln, NE). EGTA/Mg^{2+} and C1 inhibitor were from Complement Technology (Tyler, TX). Cp40 (compstatin) was generously provided by Dr. John Lambris, University of Pennsylvania, and stored as 1 mg/mL aliquots in water. Soluble CD55 (SCR1–3 of CD55) with His6 tag was expressed in *E. coli* as described by us before[41] and aliquoted at 3 mg/mL in PBS. Soluble sCR1 (SCR1–10 of CD35) was generously provided by Alexion Pharmaceuticals, Inc. (New Haven, CT) as described[51] and aliquoted at 6 mg/mL in PBS. All proteins were stored at −80 °C with less than three freeze–thaw cycles per aliquot.

METHODS

Synthesis of CLIO NWs-NH_2.

SPIO NWs and CLIO NWs were prepared by the previously described method[7,34] with some modifications. Briefly, SPIO NWs (10 mg Fe/mL in DDW) were mixed with 10 kDa PEG (100 mg/mL in DDW), epichlorohydrin, and sodium hydroxide (10N) at the volume ratio of 1:1:1:1. The mixture was stirred for 24 h at 37 °C and then stirred with ammonium (final concentration 2.5%) overnight at 4 °C. The samples were ultrafiltrated against DDW using a Pall reverse osmosis system (Pall Corp.), filtered through a 0.2 μm membrane disk filter (Millipore), and finally stored in DDW at 4 °C.

Synthesis of Fluorescently Labeled CLIO NWs-NH_2.

Aminated CLIO NWs-NH_2 (5 mg Fe/mL) were combined with a 100-fold excess of Cy5-NHS or Cy3-NHS over NWs (in 4 μL of DMSO). The reaction mixture was incubated at 4 °C for 12 h and purified using a 40 kDa cut-off Zeba spin column. Conjugation efficiency

was about ~90 fluorophores/CLIO as determined by UV absorbance and the dye extinction coefficients of 250 000 M^{-1} cm^{-1} for Cy5 and 150 000 M^{-1} cm^{-1} for Cy3.

Synthesis of MTz-PEG3400-COOH.

A mixture of NH_2-PEG3400-VA (50 mg, 0.015 mmol, 1 equiv), methyl tetrazine NHS (7.21 mg 0.022 mmol, 1.5 equiv), and DIEA (*N*,*N*-diisopropylethylamine) (8 μL, 0.044 mmol, 3 equiv) was stirred in THF at room temperature for 4 h. The solvent was then evaporated under reduced pressure, and the resulting dark pink residue was purified by using preparative HPLC and eluted with 40–50% methanol/water, to obtain MTz-PEG3400-COOH as a pink solid. Yield 68.3%. ^{1}H NMR (400 MHz, $CDCl_3$): δ 9.98 (bs, 1H, NH), 8.51 (d, J = 8.3 Hz, 2H, Ar–H), 7.48 (d, J = 8.3 Hz, 2H, Ar–H), 3.38–3.81 (m, 330H, CH_2), 3.05 (s, 3H, CH_3), 2.31 (t, J = 7.2 Hz, 2H, CH_2), 1.53–1.72 (m, 4H, CH_2).

Synthesis of Fluorescently Labeled and Nonlabeled CLIO NWs-PEG3400-MTz.

MTz-PEG3400-COOH (1.44 mg, 2000-fold molar excess), EDC (0.24 mg, 6000-fold excess), and NHS (0.15 mg, 6000-fold excess) were mixed in PBS for 30 min, and then Cy5-CLIO NWs-NH_2 (2 mg Fe) was added to the mixture. The reaction mixture was stirred at 4 °C for 12 h, then 10 000-fold excess of sulfosuccinimidyl acetate (0.5 mg) was added, and the mixture was stirred for 2 h at 4 °C. The reaction mixture was purified using a 40 kDa cut-off Zeba spin column. Nonlabeled CLIO NWs-PEG3400-MTz and Cy3-CLIO NWs-PEG3400-MTz were synthesized similarly.

Synthesis of Her-TCO and EpCAM-TCO.

Human anti-Her2/neu or anti-EpCAM in PBS (100 μL, 10 mg Fe/mL) was combined with a 10-fold excess of TCO-PEG_4-NHS (in 4 μL of DMSO). The reaction mixture was incubated at 4 °C for 12 h and purified using a 7 kDa cut-off Zebra spin column. Conjugation efficiency was about ~2 TCO/mAb as determined by UV absorbance after conjugation with Cy3-MTz and the dye extinction coefficient of 150 000 M^{-1} cm^{-1}.

Conjugation of mAb-TCO to CLIO NWs-PEG3400-MTz.

Human anti-Her2-TCO or anti-EpCAM-TCO in PBS (100 μL, 10 mg Fe/mL) at a 100-fold excess was combined with fluorescently labeled or nonlabeled CLIO NWs-PEG3400-MTz (100 μL, 5 mg/mL). The reaction mixture was incubated at 4 °C for 12 h and purified using a MACS Midi column and concentrated using 100k Amicon Ultra Centrifugal Filters. To determine the number of Abs per nanoparticle, CLIO NWs were loaded in 2 μL triplicates on a 0.45 μm nitrocellulose membrane, the membrane was blocked in 5% milk/0.1% Tween-20/PBS, and the antibody was detected with IRDye 800CW anti-human antibody. The membrane was scanned at 800 nm using Li-COR Odyssey. The integrated density of dots in 8-bit TIFF images was measured with ImageJ. Number of Abs/NP was calculated using a standard curve for the respective Ab applied on the same membrane (supplemental data). The concentration of nanoparticles used for calculations was assumed as 6×10^{13} particles per mg Fe.[33]

SKBR3 Uptake of CLIO NWs.

SKBR3 breast carcinoma cells were obtained from ATCC and maintained in McCoy's 5A medium (Corning Life Sciences, Tewksbury, MA) supplemented with 10% fetal bovine serum (FBS) (Corning Life Sciences). No more than 20 passages were allowed. To label SKBR3 cells with DiR, 2×10^7 cells were resuspended in 400 μL of 1% BSA/PBS and incubated with DiR at a 10 μM concentration for 30 min at room temperature in the dark with slow mixing. Cells were washed three times with 1% BSA/PBS at 300*g* for 5 min. Finally, the cells were resuspended in 300 μL of 1% BSA/PBS. For cell uptake experiments, 2×10^6 cells in 1% BSA/PBS or lepirudin plasma were incubated with indicated concentrations of CLIO NWs. After 1 h of incubation at 37 °C, cells were washed three times in 1% BSA/PBS. For flow cytometry analysis, cells were resuspended at ~0.5 million/mL, and 20 000 events were detected with a Guava EasyCyte HT flow cytometer (Merck KGaA). DiR fluorescence was detected in the near IR-R fluorescence channel using the red (647 nm) laser, Cy3 fluorescence was detected in the Yellow-B fluorescence channel using the blue (488 nm) laser, and Cy5 fluorescence was detected in the Red-R fluorescence channel using the red (647 nm) laser. FSC threshold was set to exclude debris. The data were analyzed using FlowJo software version V10. For internalization of particles, cells were imaged with a Zeiss Axio Observer 5 epifluorescent microscope (20× and 10× Apochromat objectives) equipped with an Exelitas near-infrared light source and five filter cubes including NIR (760 nm excitation/780 nm emission) and Axiocam 506 monochromatic camera. Alternatively, cells were imaged with a Nikon Eslipse AR1HD confocal microscope (20× Nikon Plan Apo objective).

SKBR3 Targeting in Human Blood.

Freshly drawn lepirudin anticoagulated whole human blood was spiked with DIR-labeled SKBR3 cells and incubated with nanoparticles at 37 °C with mixing. Following incubation, blood was either imaged with microscope directly on a slide or passed through a MACS Midi column and washed with 10 mL of PBS (1% BSA). The magnetic cells were eluted on a 0.45 μm nitrocellulose membrane (Bio-Rad) connected to a vacuum line. The membrane was scanned at the highest resolution (21 μm) at 800 nm using Li-COR Odyssey. For immunostaining, cells were fixed with 4% formalin, permeabilized using BD Cytoflx/Cytoperm kit for 4 h at rt, and then stained using AlexaFluor 488 labeled anti-cytokeratin antibody and AlexaFluor 594-labeled anti-CD45 antibody overnight at 4 °C. After being washed, cell nuclei were stained with DAPI/antifade media. The tumor cells "CTCs" were identified on the basis of previously published criteria,[57] including CK+/CD45-/DAPI+ staining, the presence of a defined nucleus, and dimensions larger than 4 × 4 μm. Leukocytes were identified as CK−/CD45+/DAPI+ cells.

Leukocyte and SKBR3 Uptake Efficiency Following Inhibition.

Fresh lepirudin whole blood (plain or with complement inhibitors) with or without SKBR3 cells was incubated with Cy5 labeled CLIO NWs at 37 °C for 2 h. Magnetically positive leukocytes and cells were isolated from whole human blood with MACS column and analyzed with flow cytometry or microscopy as described above. Alternatively to MACS isolation, erythrocytes were lysed with the RBC lysis buffer per the manufacturer's

instructions, and the cells were centrifuged at 200*g* for 10 min, resuspended in 1% BSA/PBS, analyzed with flow cytometry, and plotted with Prism 8 (GraphPad, San Diego, CA). The fluorescence values of cells (leukocytes and SKBR3) without particles (baseline) were subtracted from the plotted values.

Dot Blot Assay to Measure C3 Deposition.

The assay was performed as described previously.[33] Briefly, 10 μg of Fe in 10 μL of PBS was mixed with 30 μL of lepirudin plasma supplemented with inhibitors or PBS (in 2 μL volume) and incubated at 37 °C for 30 min. Particles were washed three times in 1 mL of PBS in a TLA-45 rotor (Optima Beckman ultracentrifuge) at 44 000 rpm for 8 min. Particles were resuspended in PBS, blotted as 2 μL dots on nitrocellulose membrane, and C3 was detected with anti-human C3 antibody and secondary anti-mouse IRDye800 antibody. The same amount of Fe was loaded on the membrane across the samples. The integrated density of dots was measured in triplicate and plotted in Prism 8. For IC_{50}, log-transformed concentrations of the inhibitors were plotted versus normalized responses (no inhibitor = 100%) and fitted into inhibition curves using Prism 8 software.

Statistical Analyses.

Differences in bound C3 were explored using a repeated measures three-way ANOVA model with fixed factors for type of nanoparticle, Cy5 inclusion, and type of inhibitor and random subject effects using the *lme4* (version 1.1–21)[58] and *lmerTest* (version 3.1–1)[59] packages of R Statistical Software (version 3.6.1). Pairwise differences were examined using estimated marginal means calculated using the *emmeans* package (version 1.4.4) for R. The *p*-values were adjusted for multiple testing within a research question, for example, the effect of the C1INH inhibitor for each of the nanoparticles, using a Bonferroni correction. Leukocyte uptake and SKBR3 uptake as a function of the particle type and inhibitors were analyzed in a similar manner using a repeated measure two-way ANOVA and natural log transformation of the outcomes.

Supplementary Material

Refer to Web version on PubMed Central for supplementary material.

ACKNOWLEDGMENTS

This study was supported by NIH grants EB022040 and CA194058 to D.S. We thank Dr. Lambris from the University of Pennsylvania, School of Medicine, for providing Cp40 and Alexion Pharmaceuticals Inc. (100 College St., New Haven, CT) for providing sCR1. Help from Ms. Laren Lofchy in proofreading the manuscript is gratefully acknowledged.

ABBREVIATIONS

CLIO NWs	cross-linked iron oxide nanoworms
Her2/neu	HERCEPTIN (Trastuzumab)
EpCAM	epithelial cell adhesion molecule

PEG	polyethylene glycol
SPIO	superparamagnetic iron oxide
NPs	nanoparticles
BSA	bovine serum albumin
TCO	*trans*-cyclooctene
MTz	methyltetrazine
NHS	*N*-hydroxysuccinimide
sCR1	soluble complement receptor 1
RBC	red blood cells

REFERENCES

(1). Plouffe BD, Murthy SK, and Lewis LH (2015) Fundamentals and Application of Magnetic Particles in Cell Isolation and Enrichment: A Review. Rep. Prog. Phys 78, 016601. [PubMed: 25471081]

(2). Gupta AK, and Gupta M (2005) Synthesis and Surface Engineering of Iron Oxide Nanoparticles for Biomedical Applications. Biomaterials 26, 3995–4021. [PubMed: 15626447]

(3). Wang X, and Riviere I (2016) Clinical Manufacturing of Car T Cells: Foundation of a Promising Therapy. Mol. Ther Oncolytics 3, 16015. [PubMed: 27347557]

(4). Miller MC, Doyle GV, and Terstappen LW (2010) Significance of Circulating Tumor Cells Detected by the Cellsearch System in Patients with Metastatic Breast Colorectal and Prostate Cancer. J. Oncol 2010, 617421. [PubMed: 20016752]

(5). Laurent S, Forge D, Port M, Roch A, Robic C, Vander Elst L, and Muller RN (2008) Magnetic Iron Oxide Nanoparticles: Synthesis, Stabilization, Vectorization, Physicochemical Characterizations, and Biological Applications. Chem. Rev 108, 2064–110. [PubMed: 18543879]

(6). Tassa C, Shaw SY, and Weissleder R (2011) Dextran-Coated Iron Oxide Nanoparticles: A Versatile Platform for Targeted Molecular Imaging, Molecular Diagnostics, and Therapy. Acc. Chem. Res 44, 842–52. [PubMed: 21661727]

(7). Wang G, Griffin JI, Inturi S, Brenneman B, Banda NK, Holers VM, Moghimi SM, and Simberg D (2017) In Vitro and in Vivo Differences in Murine Third Complement Component (C3) Opsonization and Macrophage/Leukocyte Responses to Antibody-Functionalized Iron Oxide Nanoworms. Front. Immunol 8, 151. [PubMed: 28239384]

(8). Wang G, Inturi S, Serkova NJ, Merkulov S, McCrae K, Russek SE, Banda NK, and Simberg D (2014) High-Relaxivity Superparamagnetic Iron Oxide Nanoworms with Decreased Immune Recognition and Long-Circulating Properties. ACS Nano 8, 12437. [PubMed: 25419856]

(9). Wunderbaldinger P, Josephson L, and Weissleder R (2002) Crosslinked Iron Oxides (Clio): A New Platform for the Development of Targeted Mr Contrast Agents. Acad. Radiol 9 (Suppl 2), S304–6. [PubMed: 12188255]

(10). Schellenberger EA, Bogdanov A Jr., Hogemann D, Tait J, Weissleder R, and Josephson L (2002) Annexin V-Clio: A Nanoparticle for Detecting Apoptosis by Mri. Mol. Imaging 1, 102–7. [PubMed: 12920851]

(11). Kircher MF, Allport JR, Graves EE, Love V, Josephson L, Lichtman AH, and Weissleder R (2003) In Vivo High Resolution Three-Dimensional Imaging of Antigen-Specific Cytotoxic T-Lymphocyte Trafficking to Tumors. Cancer Res. 63, 6838–46. [PubMed: 14583481]

(12). Chen F, Ma K, Madajewski B, Zhuang L, Zhang L, Rickert K, Marelli M, Yoo B, Turker MZ, Overholtzer M, et al. (2018) Ultrasmall Targeted Nanoparticles with Engineered Antibody

Fragments for Imaging Detection of Her2-Overexpressing Breast Cancer. Nat. Commun 9, 4141. [PubMed: 30297810]

(13). Colombo M, Fiandra L, Alessio G, Mazzucchelli S, Nebuloni M, De Palma C, Kantner K, Pelaz B, Rotem R, Corsi F, et al. (2016) Tumour Homing and Therapeutic Effect of Colloidal Nanoparticles Depend on the Number of Attached Antibodies. Nat. Commun 7, 13818. [PubMed: 27991503]

(14). Tsvetkova Y, Beztsinna N, Baues M, Klein D, Rix A, Golombek SK, Al Rawashdeh W, Gremse F, Barz M, Koynov K, et al. (2017) Balancing Passive and Active Targeting to Different Tumor Compartments Using Riboflavin-Functionalized Polymeric Nanocarriers. Nano Lett. 17, 4665–74. [PubMed: 28715227]

(15). van der Meel R, Sulheim E, Shi Y, Kiessling F, Mulder WJM, and Lammers T (2019) Smart Cancer Nanomedicine. Nat. Nanotechnol 14, 1007–17. [PubMed: 31695150]

(16). Cheng CJ, Tietjen GT, Saucier-Sawyer JK, and Saltzman WM (2015) A Holistic Approach to Targeting Disease with Polymeric Nanoparticles. Nat. Rev. Drug Discovery 14, 239–47. [PubMed: 25598505]

(17). Tietjen GT, Bracaglia LG, Saltzman WM, and Pober JS (2018) Focus on Fundamentals: Achieving Effective Nanoparticle Targeting. Trends Mol. Med 24, 598–606. [PubMed: 29884540]

(18). Moghimi SM, Andersen AJ, Ahmadvand D, Wibroe PP, Andresen TL, and Hunter AC (2011) Material Properties in Complement Activation. Adv. Drug Delivery Rev 63, 1000–07.

(19). Tavano R, Gabrielli L, Lubian E, Fedeli C, Visentin S, Polverino de Laureto P, Arrigoni G, Geffner-Smith A, Chen F, and Simberg D (2018) C1q-Mediated Complement Activation and C3 Opsonization Trigger Recognition of Stealth Poly(2-Methyl-2-Oxazoline)-Coated Silica Nanoparticles by Human Phagocytes. ACS Nano 12, 5834. [PubMed: 29750504]

(20). Inturi S, Wang G, Chen F, Banda NK, Holers VM, Wu L, Moghimi SM, and Simberg D (2015) Modulatory Role of Surface Coating of Superparamagnetic Iron Oxide Nanoworms in Complement Opsonization and Leukocyte Uptake. ACS Nano 9, 10758–68. [PubMed: 26488074]

(21). Dobrovolskaia MA, Aggarwal P, Hall JB, and McNeil SE (2008) Preclinical Studies to Understand Nanoparticle Interaction with the Immune System and Its Potential Effects on Nanoparticle Biodistribution. Mol. Pharmaceutics 5, 487–95.

(22). Salvador-Morales C, Flahaut E, Sim E, Sloan J, Green ML, and Sim RB (2006) Complement Activation and Protein Adsorption by Carbon Nanotubes. Mol. Immunol 43, 193–201. [PubMed: 16199256]

(23). Andersen AJ, Robinson JT, Dai H, Hunter AC, Andresen TL, and Moghimi SM (2013) Single-Walled Carbon Nanotube Surface Control of Complement Recognition and Activation. ACS Nano 7, 1108–19. [PubMed: 23301860]

(24). Hamad I, Hunter AC, and Moghimi SM (2013) Complement Monitoring of Pluronic 127 Gel and Micelles: Suppression of Copolymer-Mediated Complement Activation by Elevated Serum Levels of Hdl, Ldl, and Apolipoproteins Ai and B-100. J. Controlled Release 170, 167–74.

(25). Devine DV, Wong K, Serrano K, Chonn A, and Cullis PR (1994) Liposome-Complement Interactions in Rat Serum: Implications for Liposome Survival Studies. Biochim. Biophys. Acta, Biomembr 1191, 43–51.

(26). Borchard G, and Kreuter J (1996) The Role of Serum Complement on the Organ Distribution of Intravenously Administered Poly (Methyl Methacrylate) Nanoparticles: Effects of Pre-Coating with Plasma and with Serum Complement. Pharm. Res 13, 1055–8. [PubMed: 8842044]

(27). Hamad I, Al-Hanbali O, Hunter AC, Rutt KJ, Andresen TL, and Moghimi SM (2010) Distinct Polymer Architecture Mediates Switching of Complement Activation Pathways at the Nanosphere-Serum Interface: Implications for Stealth Nanoparticle Engineering. ACS Nano 4, 6629–38. [PubMed: 21028845]

(28). Dobrovolskaia MA, Patri AK, Zheng J, Clogston JD, Ayub N, Aggarwal P, Neun BW, Hall JB, and McNeil SE (2009) Interaction of Colloidal Gold Nanoparticles with Human Blood: Effects on Particle Size and Analysis of Plasma Protein Binding Profiles. Nanomedicine 5, 106–17. [PubMed: 19071065]

(29). Pedersen MB, Zhou X, Larsen EK, Sorensen US, Kjems J, Nygaard JV, Nyengaard JR, Meyer RL, Boesen T, and Vorup-Jensen T (2010) Curvature of Synthetic and Natural Surfaces Is an Important Target Feature in Classical Pathway Complement Activation. J. Immunol 184, 1931–45. [PubMed: 20053940]

(30). Wolf-Grosse S, Rokstad AM, Ali S, Lambris JD, Mollnes TE, Nilsen AM, and Stenvik J (2017) Iron Oxide Nanoparticles Induce Cytokine Secretion in a Complement-Dependent Manner in a Human Whole Blood Model. Int. J. Nanomed 12, 3927–40.

(31). Slamon D, Eiermann W, Robert N, Pienkowski T, Martin M, Press M, Mackey J, Glaspy J, Chan A, Pawlicki M, et al. (2011) Adjuvant Trastuzumab in Her2-Positive Breast Cancer. N. Engl. J. Med 365, 1273–83. [PubMed: 21991949]

(32). Rao CG, Chianese D, Doyle GV, Miller MC, Russell T, Sanders RA Jr., and Terstappen LW (2005) Expression of Epithelial Cell Adhesion Molecule in Carcinoma Cells Present in Blood and Primary and Metastatic Tumors. Int. J. Oncol 27, 49–57. [PubMed: 15942643]

(33). Benasutti H, Wang G, Vu VP, Scheinman R, Groman E, Saba L, and Simberg D (2017) Variability of Complement Response toward Preclinical and Clinical Nanocarriers in the General Population. Bioconjugate Chem. 28, 2747–55.

(34). Wang G, Chen F, Banda NK, Holers VM, Wu L, Moghimi SM, and Simberg D (2016) Activation of Human Complement System by Dextran-Coated Iron Oxide Nanoparticles Is Not Affected by Dextran/Fe Ratio, Hydroxyl Modifications, and Crosslinking. Front. Immunol 7, 418. [PubMed: 27777575]

(35). McKay CS, and Finn MG (2014) Click Chemistry in Complex Mixtures: Bioorthogonal Bioconjugation. Chem. Biol 21, 1075–101. [PubMed: 25237856]

(36). Subik K, Lee JF, Baxter L, Strzepek T, Costello D, Crowley P, Xing L, Hung MC, Bonfiglio T, Hicks DG, et al. (2010) The Expression Patterns of Er, Pr, Her2, Ck5/6, Egfr, Ki-67 and Ar by Immunohistochemical Analysis in Breast Cancer Cell Lines. Breast Cancer: Basic Clin. Res 4, 35–41.

(37). Kraeft SK, Ladanyi A, Galiger K, Herlitz A, Sher AC, Bergsrud DE, Even G, Brunelle S, Harris L, Salgia R, et al. (2004) Reliable and Sensitive Identification of Occult Tumor Cells Using the Improved Rare Event Imaging System. Clin. Cancer Res 10, 3020–8. [PubMed: 15131038]

(38). Bauer KD, de la Torre-Bueno J, Diel IJ, Hawes D, Decker WJ, Priddy C, Bossy B, Ludmann S, Yamamoto K, Masih AS, et al. (2000) Reliable and Sensitive Analysis of Occult Bone Marrow Metastases Using Automated Cellular Imaging. Clin. Cancer Res 6, 3552–9. [PubMed: 10999743]

(39). Krivacic RT, Ladanyi A, Curry DN, Hsieh HB, Kuhn P, Bergsrud DE, Kepros JF, Barbera T, Ho MY, Chen LB, et al. (2004) A Rare-Cell Detector for Cancer. Proc. Natl. Acad. Sci. U. S. A 101, 10501–4. [PubMed: 15249663]

(40). Tveito S, Maelandsmo GM, Hoifodt HK, Rasmussen H, and Fodstad O (2007) Specific Isolation of Disseminated Cancer Cells: A New Method Permitting Sensitive Detection of Target Molecules of Diagnostic and Therapeutic Value. Clin. Exp. Metastasis 24, 317–27. [PubMed: 17530423]

(41). Gifford G, Vu VP, Banda NK, Holers VM, Wang G, Groman EV, Backos D, Scheinman R, Moghimi SM, and Simberg D (2019) Complement Therapeutics Meets Nanomedicine: Overcoming Human Complement Activation and Leukocyte Uptake of Nanomedicines with Soluble Domains of Cd55. J. Controlled Release 302, 181–89.

(42). Chen F, Wang G, Griffin JI, Brenneman B, Banda NK, Holers VM, Backos DS, Wu L, Moghimi SM, and Simberg D (2017) Complement Proteins Bind to Nanoparticle Protein Corona and Undergo Dynamic Exchange in Vivo. Nat. Nanotechnol 12, 387–93. [PubMed: 27992410]

(43). Fries LF, Gaither TA, Hammer CH, and Frank MM (1984) C3b Covalently Bound to Igg Demonstrates a Reduced Rate of Inactivation by Factors H and I. J. Exp. Med 160, 1640–55. [PubMed: 6239898]

(44). Venkatesh YP, Minich TM, Law SK, and Levine RP (1984) Natural Release of Covalently Bound C3b from Cell Surfaces and the Study of This Phenomenon in the Fluid-Phase System. J. Immunol 132, 1435–9. [PubMed: 6693771]

(45). Vu VP, Gifford GB, Chen F, Benasutti H, Wang G, Groman EV, Scheinman R, Saba L, Moghimi SM, and Simberg D (2019) Immunoglobulin Deposition on Biomolecule Corona Determines Complement Opsonization Efficiency of Preclinical and Clinical Nanoparticles. Nat. Nanotechnol 14, 260–68. [PubMed: 30643271]

(46). Forneris F, Wu J, Xue X, Ricklin D, Lin Z, Sfyroera G, Tzekou A, Volokhina E, Granneman JCM, Hauhart R, et al. (2016) Regulators of Complement Activity Mediate Inhibitory Mechanisms through a Common C3b-Binding Mode. EMBO J. 35, 1133–49. [PubMed: 27013439]

(47). Smith GP, and Smith RA (2001) Membrane-Targeted Complement Inhibitors. Mol. Immunol 38, 249–55. [PubMed: 11532286]

(48). Risitano AM, Ricklin D, Huang Y, Reis ES, Chen H, Ricci P, Lin Z, Pascariello C, Raia M, Sica M, et al. (2014) Peptide Inhibitors of C3 Activation as a Novel Strategy of Complement Inhibition for the Treatment of Paroxysmal Nocturnal Hemoglobinuria. Blood 123, 2094–101. [PubMed: 24497537]

(49). Mastellos DC, Yancopoulou D, Kokkinos P, Huber-Lang M, Hajishengallis G, Biglarnia AR, Lupu F, Nilsson B, Risitano AM, Ricklin D, et al. (2015) Compstatin: A C3-Targeted Complement Inhibitor Reaching Its Prime for Bedside Intervention. Eur. J. Clin. Invest 45, 423–40. [PubMed: 25678219]

(50). Risitano AM, Ricklin D, Huang YJ, Reis ES, Chen H, Ricci P, Lin ZE, Pascariello C, Raia M, Sica M, et al. (2014) Peptide Inhibitors of C3 Activation as a Novel Strategy of Complement Inhibition for the Treatment of Paroxysmal Nocturnal Hemoglobinuria. Blood 123, 2094–101. [PubMed: 24497537]

(51). Fridkis-Hareli M, Storek M, Or E, Altman R, Katti S, Sun F, Peng T, Hunter J, Johnson K, Wang Y, et al. (2019) The Human Complement Receptor Type 2 (Cr2)/Cr1 Fusion Protein Tt32, a Novel Targeted Inhibitor of the Classical and Alternative Pathway C3 Convertases, Prevents Arthritis in Active Immunization and Passive Transfer Mouse Models. Mol. Immunol 105, 150–64. [PubMed: 30513451]

(52). de la Harpe KM (2019) The Hemocompatibility of Nanoparticles. Cells 8, 1209.

(53). Wolfram J, Zhu M, Yang Y, Shen J, Gentile E, Paolino D, Fresta M, Nie G, Chen C, Shen H, et al. (2015) Safety of Nanoparticles in Medicine. Curr. Drug Targets 16, 1671–81. [PubMed: 26601723]

(54). Morgan BP, and Harris CL (2015) Complement, a Target for Therapy in Inflammatory and Degenerative Diseases. Nat. Rev. Drug Discovery 14, 857–77. [PubMed: 26493766]

(55). Barnum SR (2017) Therapeutic Inhibition of Complement: Well Worth the Risk. Trends Pharmacol. Sci 38, 503–05. [PubMed: 28413098]

(56). Ruan HH, Scott KR, Bautista E, and Ammons WS (2003) Ing-1(Hemab), a Monoclonal Antibody to Epithelial Cell Adhesion Molecule, Inhibits Tumor Metastases in a Murine Cancer Model. Neoplasia 5, 489–94. [PubMed: 14965442]

(57). Allard WJ, Matera J, Miller MC, Repollet M, Connelly MC, Rao C, Tibbe AGJ, Uhr JW, and Terstappen LWMM (2004) Tumor Cells Circulate in the Peripheral Blood of All Major Carcinomas but Not in Healthy Subjects or Patients with Nonmalignant Diseases. Clin. Cancer Res 10, 6897–904. [PubMed: 15501967]

(58). Bates D, Mächler M, Bolker B, and Walker S (2015) Fitting linear mixed-effects models using Lme4. J. Stat. Softw 1, 1 DOI: 10.18637/jss.v067.i01.

(59). Kuznetsova A, Brockhoff PB, and Christensen RHB (2017) Lmertest package: Tests in linear mixed effects models. J. Stat. Softw 1, 1 DOI: 10.18637/jss.v082.i13.

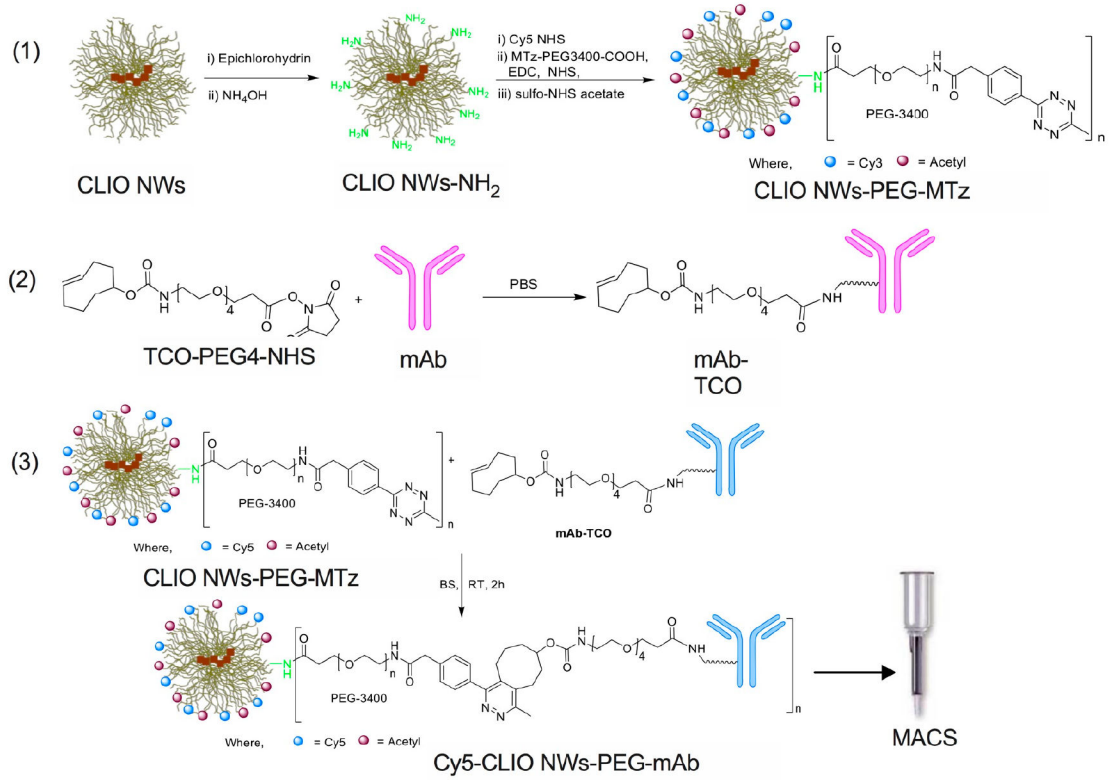

Figure 1.

Synthesis of targeted CLIO NWs. Synthetic steps: (1) Conjugation of methyltetrazine (MTz) PEG to CLIO NWs. Aminated CLIO NWs were synthesized from dextran SPIO NWs as described.[34] (2) Synthesis of *trans*-cyclooctene (TCO) modified IgG. (3) Click reaction and nanoparticle purification.

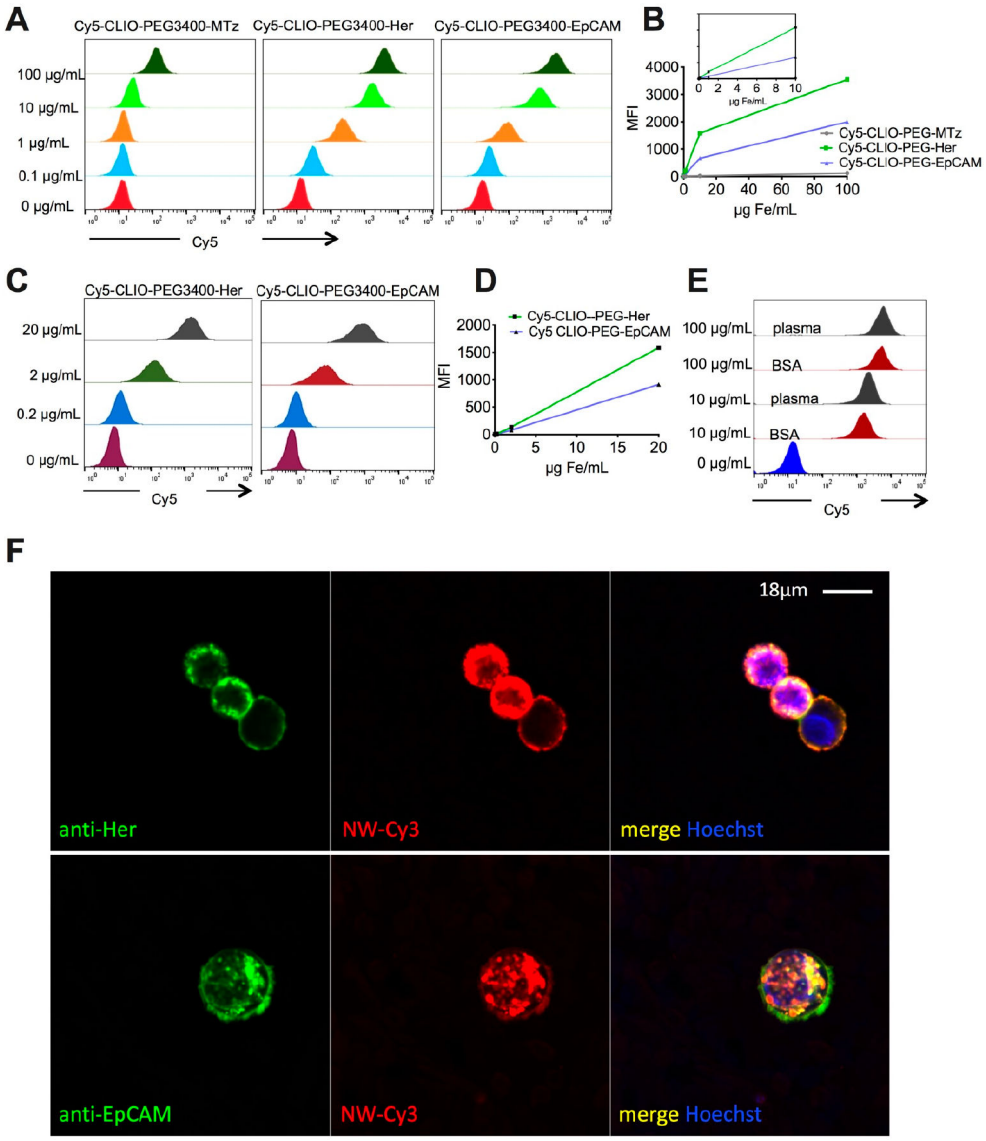

Figure 2.

Validation of targeting efficiency in BSA and plasma. (A) Flow cytometry analysis shows antibody-conjugated CLIO NWs binding to SKBR3 cells in 10 mg/mL BSA and low binding of nontargeted CLIO NWs. (B) Mean fluorescence of cells. Inset shows the linear increase between 0.1 and 10 μg/mL. (C) Flow cytometry analysis of binding to SKBR3 cells in lepirudin plasma. (D) Linear increase in the binding between 0.2 and 10 μg/mL. (E) Side-by-side comparison of binding of Cy5-CLIO NWs-PEG-Her in 10 mg/mL BSA and plasma shows no difference in targeting efficiency. (F) Confocal microscopy shows uptake of Cy3-CLIO-PEG-Her2-Cy5 and Cy3-CLIO-PEG-EpCAM-Cy5 by SKBR3 cells in 10 mg/mL BSA. Nanoparticles are localized on the membrane and inside the cells.

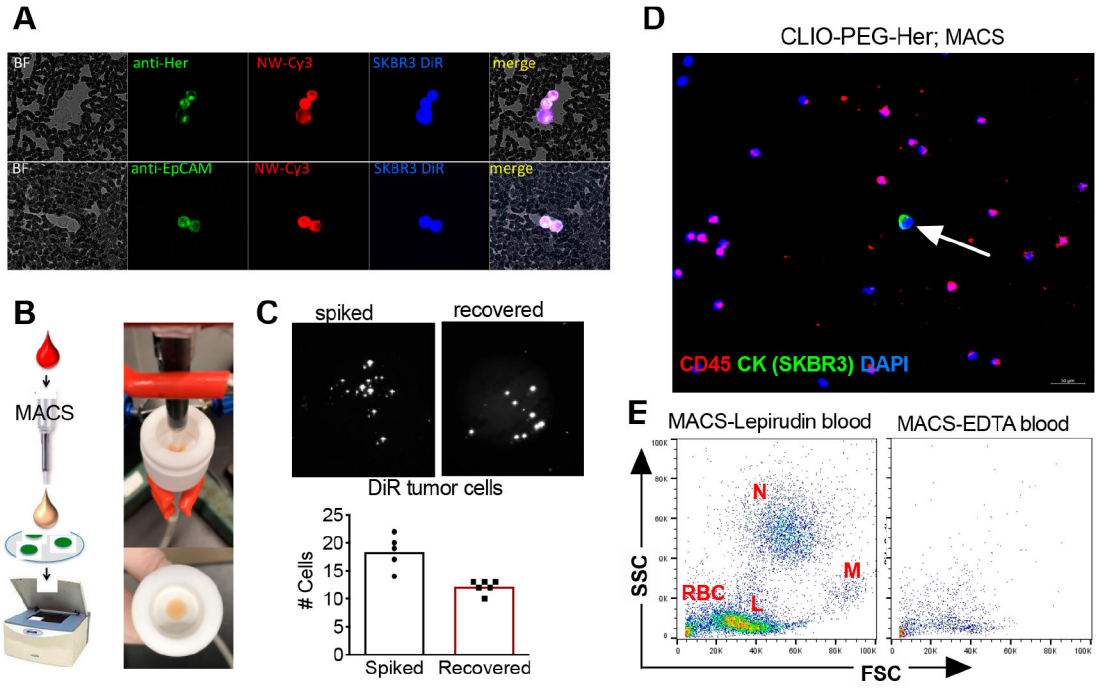

Figure 3.

Targeted CLIO NWs are efficiently taken up by tumor cells, but also by leukocytes in lepirudin blood. (A) Fluorescent microscopy of whole blood smear following incubation of targeted CLIO NWs in lepirudin anticoagulated blood shows that DiR-labeled SKBR3 cells internalized Cy3-CLIO NWs-PEG-Her-Cy5 and Cy3-CLIO NWs-PEG-EpCAM-Cy5 (1 μg/mL, 15 min incubation). (B) MACS setup for isolation and capture of magnetically labeled blood cells and detection of DIR-labeled tumor cells on a nitrocellulose membrane with Li-COR Odyssey. (C) DiR-labeled SKBR3 cells (spiked ~18 cells per 5 mL of blood) were isolated with CLIO NW-PEG-Her and scanned with Li-COR as described in the Methods. The same number of spiked cells was added directly to membrane as a loading control and scanned along with the isolated cells. Each bright dot is a DiR labeled cell. The presence of the cells was confirmed via fluorescent microscopy (not shown). The graph shows a summary of two independent experiments in triplicate. (D) Numerous leukocytes were coeluted together with tumor cell (arrow) from MACS column. CK (cytokeratin) labels tumor cells, CD45 antibody labels leukocytes, and DAPI stains nuclei. Size bar 50 μm. (E) Flow cytometry analysis (forward scattering-side scattering plot) of MACS eluted blood cells shows neutrophils (N), monocytes (M), lymphocytes (L), and red blood cells (RBCs). The same experiment in EDTA anticoagulated blood showed a dramatic decrease in MACS eluted cells, which suggested the involvement of complement. A representative experiment out of three is shown.

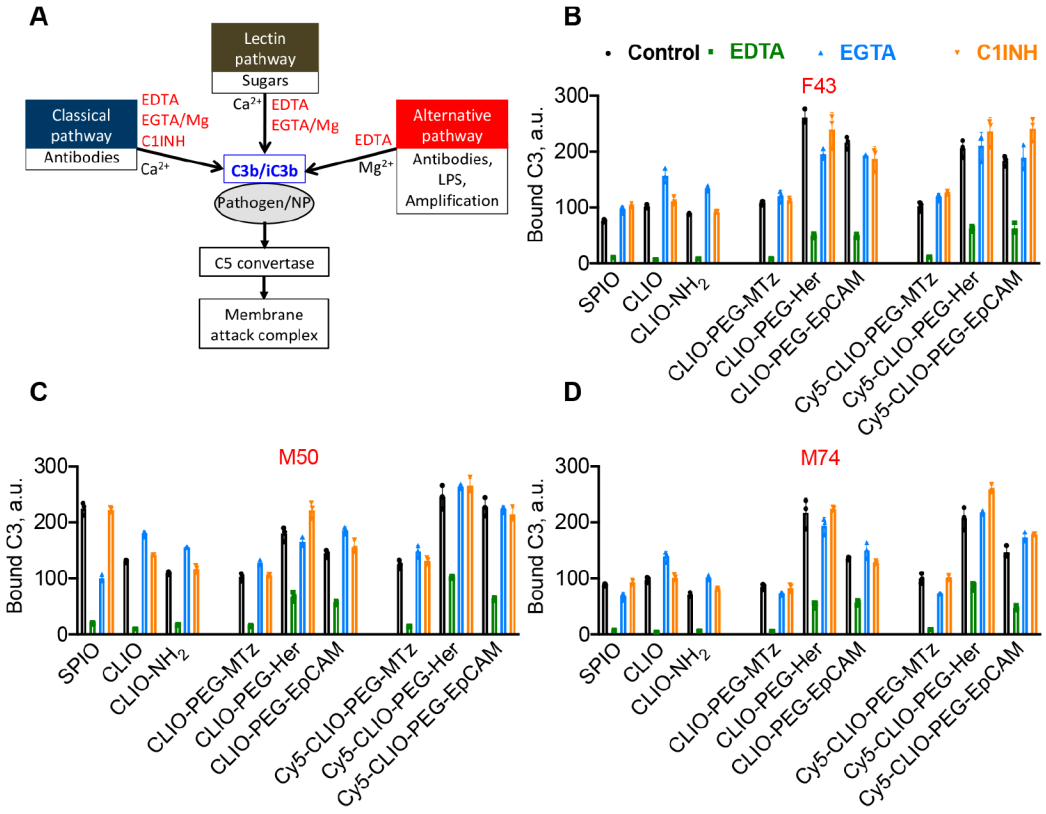

Figure 4.

Comprehensive analysis of complement C3 opsonization pathways as a function of surface properties of NWs. (A) Complement activation can be inhibited by 10 mM EDTA (all pathways), 10 mM EGTA/Mg^{2+} (classical and lectin pathway), or C1INH (classical pathway). (B) Formulations described in Table 1 were incubated in plasma from three donors (two males and one female). C3 deposition was directly measured with dot blot assay (one female and two males; age and gender are shown in red above each graph). All particles activate complement via the AP with no involvement of the CP. Conjugation of targeting antibodies increases C3 deposition. EDTA does not fully inhibit C3 deposition on targeted CLIO NWs, which suggests that some C3 binds to IgG without complement activation. Data show triplicates with mean and SD. Details of statistical analysis are given in the Methods.

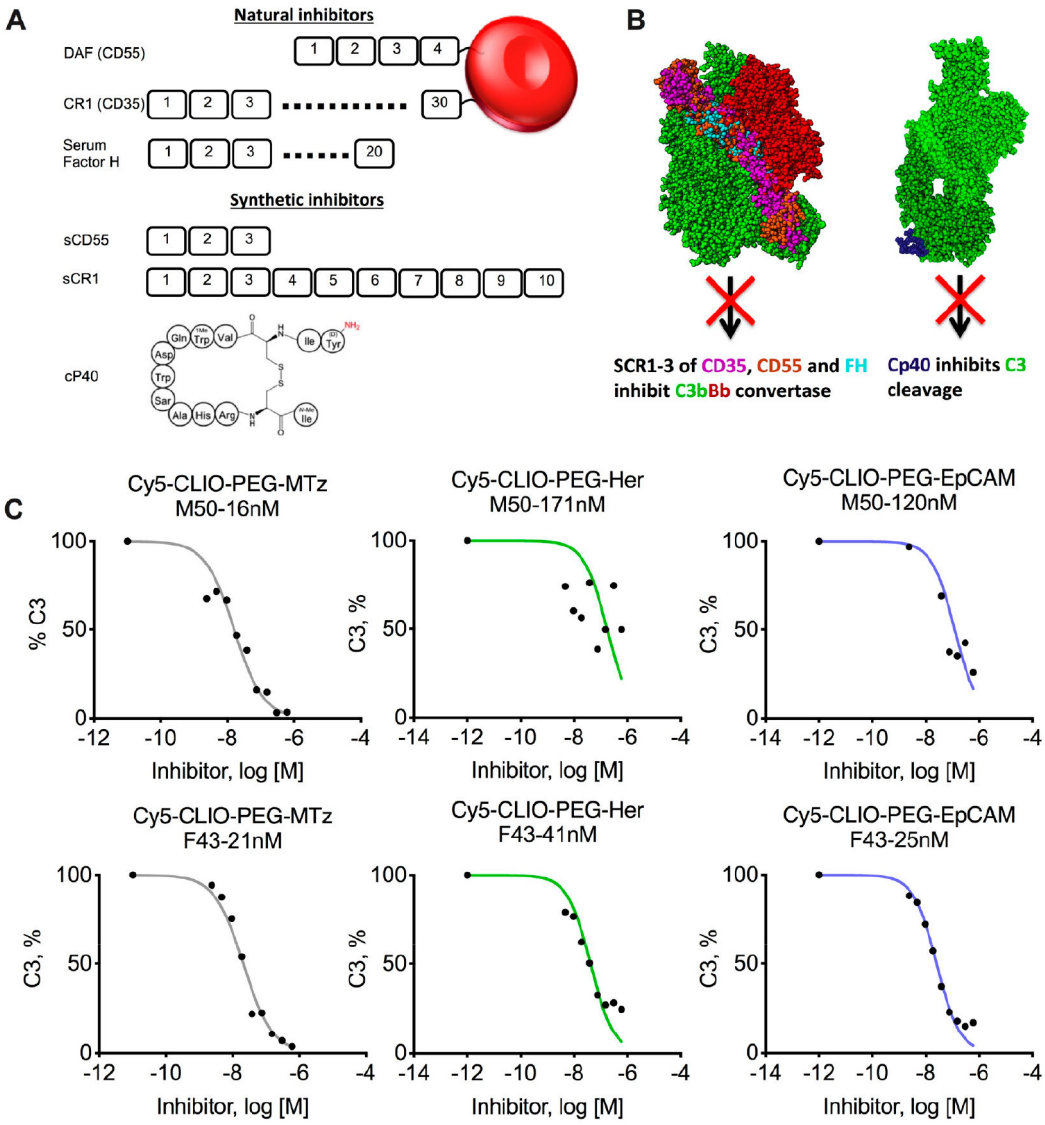

Figure 5.

Complement therapeutics for inhibition of opsonization of CLIO NWs. (A) Top, cell membrane-anchored complement control proteins CD35 and CD55 and their soluble serum counterpart FH. Each protein is composed of short consensus repeats (SCRs). Bottom, short synthetic derivatives sCD55 and sCR1 and the cyclic peptide inhibitor Cp40 (compstatin, adopted from ref 48). (B) Mechanisms of action of the inhibitors. Left, three N-terminal SCRs of CD55, CD35, and FH accelerate the disassembly (decay) of the AP convertase. The crystal structure of the C3b-FH complex (PDB ID: 2WII) was superimposed with CD55 (PDB ID: 1OJV) and CD35 (PDB ID: 1GKG) on the basis of sequence similarity as described previously.[41] Right, Cp40 binds to C3 and prevents cleavage by convertases. For the C3-compstatin complex, PDB ID 1A1P (compstatin) and PDB ID 2A73 (C3) were aligned as described.[49] (C) Inhibition of C3 opsonization of nontargeted and targeted CLIO NWs by sCR1 in two plasma donors (one male and one female; gender, age, and IC_{50} values

are shown above each graph). Targeted CLIO NWs show residual C3 deposition at micromolar concentrations of the inhibitor.

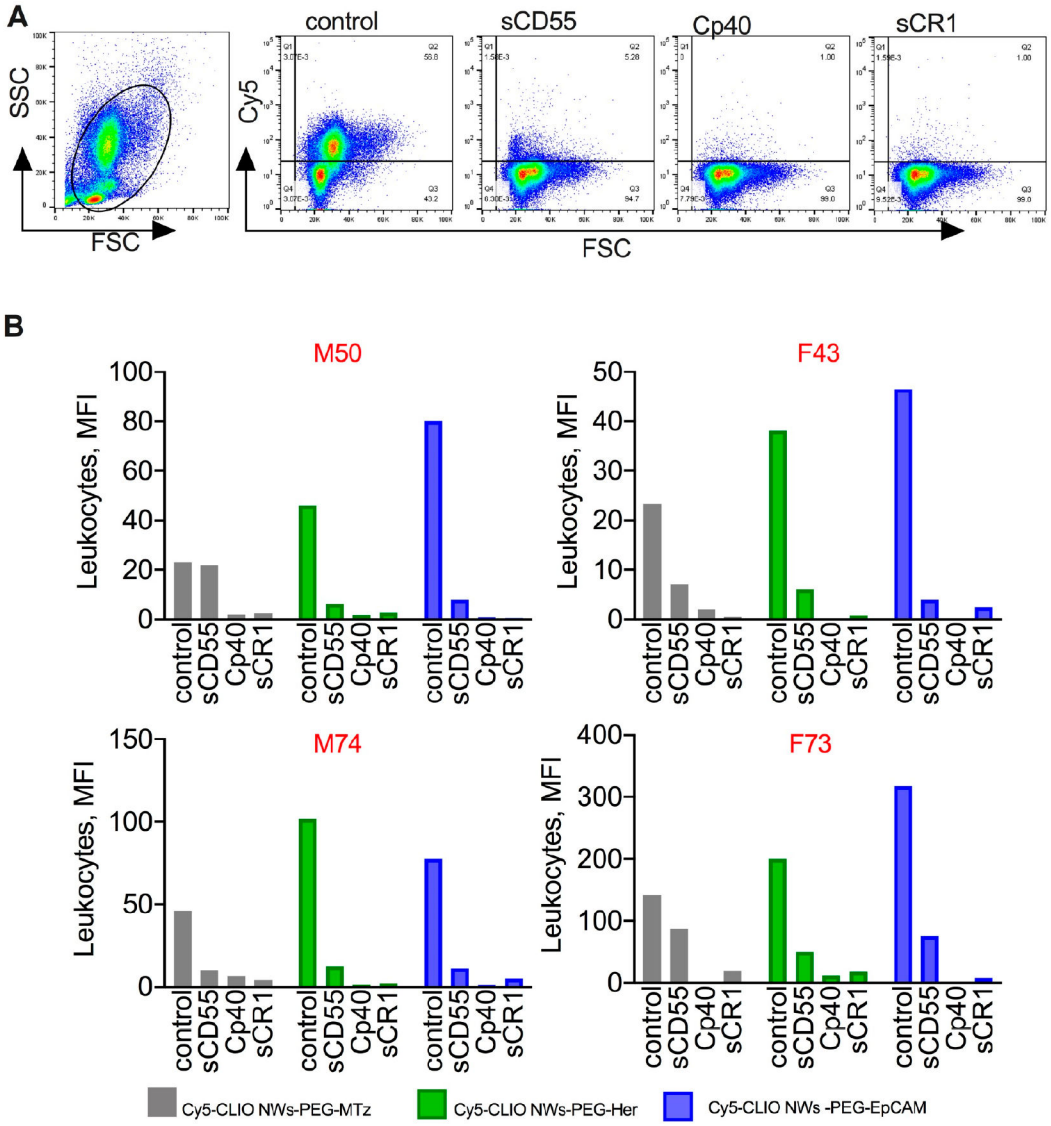

Figure 6.

Inhibition of leukocyte uptake by soluble complement inhibitors: Nontargeted and targeted Cy5-CLIO NWs were incubated in blood at 2 μg/mL with or without inhibitors (30 μg/mL), and the uptake was determined with flow cytometry after RBC lysis. (A) Representative dot plots show inhibition of the leukocyte uptake of Cy5-CLIO NWs-PEG-Her. (B) Summary of the leukocyte uptake in blood of four healthy donors (two males and two females; gender and age are shown above each graph). There was a significant decrease by sCD55, sCR1, and Cp40 for all particles, but sCR1 and Cp40 were more effective. Details of statistical analysis are given in the Methods.

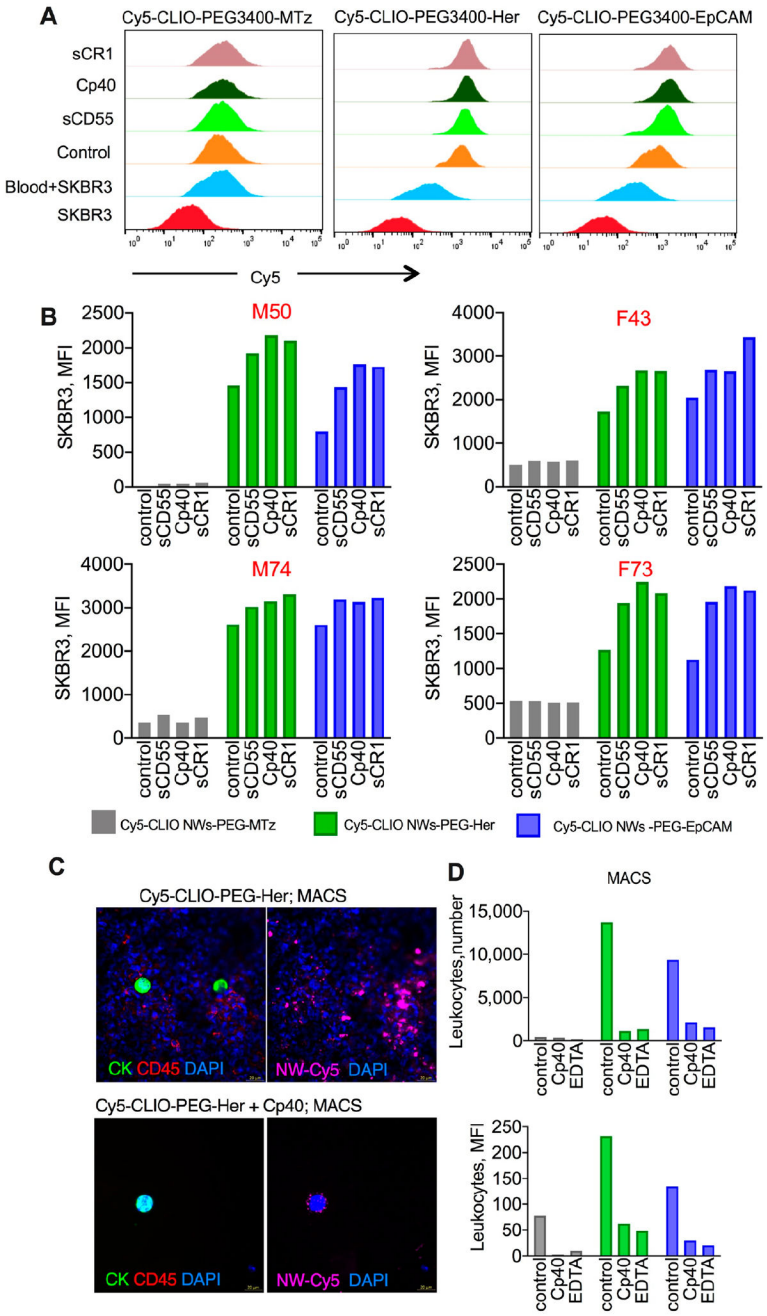

Figure 7.

Complement inhibitors increase targeting selectivity and improve purity of magnetic isolation. DiR-labeled SKBR3 cells were spiked into aliquots of lepirudin blood used for experiments in Figure 6 (~100 000 cells/mL), and the uptake of targeted and nontargeted Cy5-CLIO NWs (2 μg/mL) was determined. (A) Representative histograms of SKBR3 mean fluorescence after lysis of RBCs and gating out leukocytes (Figure S4). SKBR3 and "blood +SKBR3" are samples without added particles. (B) Summary of experiments in the blood of four healthy donors (two males and two females; gender and age are shown above each graph). There was no decrease in the uptake of targeted CLIO NWs after addition of the

inhibitors. (C) Rare SKBR3 cells were spiked in lepirudin blood (~30 cells/mL) and isolated with MACS using Cy5-CLIO NWs-EpCAM (10 μg/mL) with or without 30 μg/mL Cp40 as described in Figure 3. Immunostaining of the membrane shows single tumor cells and a decrease in contaminating leukocytes (CK−/CD45+/DAPI+) by Cp40. Size bar 20 μm. (D) Flow cytometry analysis of leukocytes eluted from MACS column with or without Cp40 shows a decrease in the number of magnetically labeled leukocytes and mean fluorescence intensity for nontargeted and targeted CLIO NWs (10 μg/mL). Repeated twice.

Table 1.

Derivatives of NWs Used in This Study[a]

nanoworm type	no. of Cy5 used	no. of PEG3400-MTz used	no. of mAb used	no. of mAb conjugated	zeta (mV)	size (nm)	PDI
SPIO NWs					−5.35 ± 0.215	62.25 ± 0.246	0.204
CLIO NWs					−5.44 ± 0.273	51.10 ± 0.225	0.121
CLIO NWs-NH					15.20 ± 0.265	55.55 ± 0.258	0.141
CLIO NWs-PEG3400-MTz		2000			−2.86 ± 0.228	57.23 ± 1.624	0.196
CLIO NWs-PEG3400-Her2		2000	100	72	−3.42 ± 0.302	71.30 ± 1.329	0.265
CLIO NWs-PEG3400-EpCAM		2000	100	57	−4.08 ± 0.596	60.72 ± 0.241	0.123
Cy5-CLIO NWs-PEG3400-MTz	100	2000			−2.60 ± 0.237	56.72 ± 0.317	0.156
Cy5-CLIO NWs-PEG3400-Her2	100	2000	100	75	−2.35 ± 0.591	62.51 ± 0.315	0.141
Cy5-CLIO NWs-PEG3400-EpCAM	100	2000	100	60	−3.75 ± 0.153	60.25 ± 0.247	0.136

[a]Size and zeta potentials show the average and the standard deviation of three independent measurements. Additional particles used throughout this study are shown in the Supporting Information.